Thermophysical behavior of thermal sprayed yttria stabilized zirconia based composite coatings

Nath, S, Manna, I, Jha, AK, Sharma, SC, Pratihar, SK & Dutta Majumdar, J

Author's Accepted Manuscript

Thermophysical Behavior of Thermal Sprayed Yttria Stabilized Zirconia Based Composite Coatings

S. Nath, I. Manna, A.K. Jha, S.C. Sharma, S.K. Pratihar, J. Dutta Majumdar
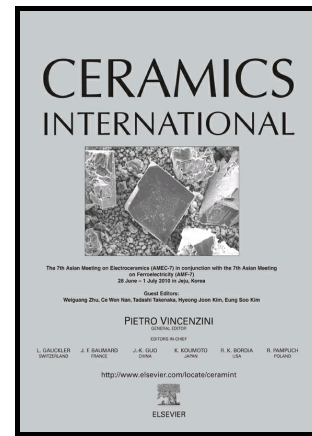
Cite this article as: S. Nath, I. Manna, A.K. Jha, S.C. Sharma, S.K. Pratihar and J. Dutta Majumdar, Thermophysical Behavior of Thermal Sprayed Yttria Stabilized Zirconia Based Composite Coatings, *Ceramics International*, http://dx.doi.org/10.1016/j.ceramint.2017.05.170

This is a PDF file of an unedited manuscript that has been accepted for publication. As a service to our customers we are providing this early version of the manuscript. The manuscript will undergo copyediting, typesetting, and review of the resulting galley proof before it is published in its final citable form. Please note that during the production process errors may be discovered which could affect the content, and all legal disclaimers that apply to the journal pertain.

Thermophysical Behavior of Thermal Sprayed Yttria Stabilized Zirconia Based Composite Coatings

S. Nath[a], I. Manna[b,c], A. K. Jha[d], S. C. Sharma[d], S. K. Pratihar[e], J. Dutta Majumdar[b*]

[a]Department of Mechanical, Aerospace and Automotive Engineering, Coventry University, Coventry CV1 2JH, United Kingdom

[b]Department of Metallurgical and Materials Engineering, Indian Institute of Technology, Kharagpur 721302, West Bengal, India

[c]Indian Institute of Technology, Kanpur 208016, Uttar Pradesh, India

[d]Vikram Sarabhai Space Centre (VSSC), Thiruvananthapuram - 695 022

[e]Department of Ceramic Engineering, National Institute of Technology, Rourkela 769008, Odisha, India

subhasisa.nath@coventry.ac.uk

imanna@iitkgp.ac.in

ak_jha@vssc.gov.in

sharma_sc@vssc.gov.in

skpratihar@nitrkl.ac.in

jyotsna@metal.iitkgp.ernet.in

[*]Corresponding author: FAX: +91-3222-282280

Abstract

The effective thermal conductivity of a composite coating depends on intrinsic thermal conductivity of the constituent phases, its characteristics (size, shape) and area fraction of porosities. The present study concerns studying the effect of CoNiCrAlY and Al_2O_3 content on the coefficient of thermal expansion and thermal conductivity of the YSZ (YSZ-CoNiCrAlY and YSZ- Al_2O_3) based composite coatings developed by thermal spray deposition technique. The coefficient of thermal expansion and thermal conductivity of the composite coatings were measured by push rod dilatometer and laser flash techniques, respectively, from room temperature to 1000 °C. Variation in density, porosity, coefficient of thermal expansion, and thermal conductivity was observed in the composite coatings with the addition of different volume fraction of CoNiCrAlY and Al_2O_3 powders in YSZ-CoNiCrAlY and YSZ-Al_2O_3 composites, respectively. Comparison between the theoretical and experimental thermal conductivities showed a mismatch varying from 4% to 58% for YSZ-CoNiCrAlY composite coatings and from 58% to 80% for YSZ- Al_2O_3 composite coatings. Model based analyses were

used to understand the mechanism of thermal conductivity reduction in the composite coatings. It was concluded that the morphology of porosities varied with composition.

1.   Introduction

Thermal barrier coatings (TBCs) are useful in protecting and extending the operational life of the gas turbine engine components (burners, transition ducts, blades, and vanes) which are exposed to corrosive and oxidative environments operated at elevated temperature [1, 2]. The efficiency of a turbine engine may be improved by increasing the turbine inlet temperature, and increasing the life of the coated component.

Conventional TBC consists of a two layer coatings where, the ceramic top coat (YSZ) is deposited on to the surface of pre-deposited bond coat (MCrAlY, M= Co, Ni, or both). Though, the superior thermal shock resistance of the Yttria stabilized Zirconia (YSZ) coating makes it a popular material for TBC application, however, the mismatch in the coefficient of thermal expansion (CTE) between the top coat and bond coat is the major cause of failure of TBC under cyclic environment [3,4]. To minimize the failure due to coefficient of thermal expansion (CTE) mismatch, in a MCrAlY/YSZ duplex TBC, and a MCrAlY/YSZ functionally graded thermal barrier coating (FGTBC) has been proposed [4-10]. YSZ/Al$_2$O$_3$ composite coatings have also been reported to improve the hot corrosion resistance and oxidation resistance of TBC [11-14]. Presence of Al$_2$O$_3$ phase in the YSZ/Al$_2$O$_3$ composite coating is beneficial in improving its thermal cycling resistance, hot corrosion and oxidation resistance properties [11-13]. However, a detailed study of the thermal properties of YSZ/Al$_2$O$_3$ composite coating has not been

1

undertaken. Thermal conductivity of any material is an important parameter which allows a quantitative as well as qualitative assessment of the heat transfer characteristics of the material. A significant reduction in thermal conductivity can be achieved by the introduction of microstructural defects in the form of porosities, micro-cracks, and interfaces. Yang et al. [15] compared the experimentally measured thermal conductivity of the sintered YSZ/Al$_2$O$_3$ composites with its theoretical value to conclude on the role of interfacial thermal resistance on the effective thermal conductivity of the composites [15]. The deviation of the thermal conductivity from its intrinsic value is not only dependent on the content of porosity in the coating but also on its morphology [16-18]. In a composite coating, the morphology and area fraction of the pores are dependent on the constituent phases present in the microstructure as they alter the effective thermal conductivity of the composite coatings. Process parameters also have a strong influence on the melting behavior of the powder particles during thermal spray deposition as they control the in-flight particle state (temperature and velocity) and hence, the microstructure [19]. Hence, engineering the composition as well as microstructure is a biggest challenge to enhance the service life of the coated component.

It is well understood that the inter-lamellar porosities have a dominant role in reducing the thermal conductivity more effectively than that of globular porosities due to the presence of porosities aligned perpendicular to the direction of heat flow. It is also reported that the morphology and orientation of porosities in the coating change the effective thermal conductivity of the thermal spray coatings [16-18]. The analyses are based on the available analytical models for different pore shapes [20-22]. From the reported results, it may be concluded that analytical models are helpful in establishing an understanding between microstructural features (structure) and thermal conductivity (property). Though, the reported results were based on the analysis of

the 100% ceramic coatings, however, no discussions are available concerning the effect of composition (e.g. composite coatings) on the morphology of porosities and hence, the thermal conductivity behavior. Bakshi et al [18] studied the thermal conductivity of the multi-walled carbon nanotubes (MWNT) - Al_2O_3 composite coatings with varying MWNT content developed by plasma spray method and reported a good match between the theoretical thermal conductivity, calculated by the available theoretical models, and experimentally measured values for some models and poor match for others. However, extensive studies need to be undertaken to address the composition induced change in morphology of pores developed by thermal spray deposition technique.

In the present study, composite coatings consisting of CoNiCrAlY-YSZ and YSZ-Al_2O_3 have been developed by thermal spray deposition technique. The thermal properties such as coefficient of thermal expansion and thermal conductivity of the composite coatings have been measured to understand the effect of composition on the thermal properties of the composite coatings. Finally, analytical model based thermal conductivity analyses have been undertaken to understand the effect of composition on the pore morphology which is a matter of immense importance owing to the fact that the pore morphology significantly alters the effective thermal conductivity of the composite coating.

2. Experimental

2.1. Materials

Commercially available CoNiCrAlY alloy powder (Co-32Ni-21Cr-8Al-0.5Y in wt.%, MEC 9950AM, particle size 15-45 μm), yttria stabilized zirconia (7 wt% Y_2O_3-ZrO_2, Amperit 831.007, particle size 15-85 μm) and Al_2O_3 (Amperit 740.1, particle size 22-45 μm) ceramic

3

powders were used as feedstock powders for the development of CoNiCrAlY-YSZ and YSZ-Al$_2$O$_3$ composite coatings. Fig. 1 shows the scanning electron micrographs of (a) YSZ, (b) Al$_2$O$_3$, and (c) CoNiCrAlY powders used as feedstock for the development of CoNiCrAlY-YSZ and YSZ-Al$_2$O$_3$ composite coatings. The shape of YSZ and CoNiCrAlY powders are spherical which ensure good flow characteristics of the powder particles. On the other hand, the Al$_2$O$_3$ powder is irregular in shape due to the partial ionic bonding characteristics and a typical powder processing route. Fig. 2 shows the X-ray diffraction profiles of (a) YSZ, (b) Al$_2$O$_3$, and (c) CoNiCrAlY feedstock powders. The X -ray diffraction profiles of YSZ (Fig. 2a) and Al$_2$O$_3$ (Fig. 2b) feedstock powders show presence of single phase tetragonal zirconia (t′–ZrO$_2$) and α–Al$_2$O$_3$, respectively. On the other hand, the X-ray diffraction profile of CoNiCrAlY powder (Fig. 2c) shows the presence of γ′ -Ni$_3$Al and β –CoAl phases in γ –Co matrix. The β –CoAl phase acts as an aluminum reservoir which helps in the formation of Al$_2$O$_3$ scales during high temperature exposure of TBC.

2.2. Development of composite coatings

Prior to thermal spray deposition, the substrates were grit blasted using alumina grits followed by simultaneous cleaning in acetone and isopropyl alcohol. For the development of CoNiCrAlY/ YSZ composite coatings, CoNiCrAlY and YSZ powders were initially mixed in the volume ratio of 70:30, 50:50, and 30:70 using a planetary ball mill for 4 hours at 300 rpm to ensure proper mixing of powders without altering their original shapes. The 100% CoNiCrAlY and 100% YSZ coatings were deposited on the grit blasted substrates using high velocity oxy-fuel spray (HVOF) and atmospheric plasma spray (APS) techniques, respectively. Similarly, for the development of YSZ-Al$_2$O$_3$ composite coatings, Al$_2$O$_3$ and YSZ powders were mixed in the volume ratio of

4

70:30, 50:50, and 30:70 using a planetary ball mill for 4 hours at 300 rpm to ensure proper mixing of powders. Table I summarizes the process parameters employed for the plasma spray deposition of composite coatings.

2.3. Characterization of thermal barrier coatings

Followed by the development of coating, a detailed characterization of the microstructure of the coated surface was carried out by field emission scanning electron microscopy (SUPRA 40, Zeiss SMT AG, Germany). The grain size of the YSZ and Al2O3 coatings were measured by linear intercept method (ASTM E112). A detailed phase analysis of the coating was carried out by X-ray diffraction (XRD) technique (Bruker D8 Discover, Germany) using Cu Kα radiation (wavelength ~ 0.15418 nm) at a scanning speed of 0.05°/s. The X-ray source was operated at an accelerating voltage of 40 kV and current of 40 mA.

Free standing coatings of CoNiCrAlY/YSZ were obtained by depositing the coatings onto the polished steel substrates followed by carefully cutting out the coating using a slow speed diamond cutter. On the other hand, YSZ- Al_2O_3 composite coatings were deposited onto the polished steel substrates followed by immersing it in a 40% HNO_3 solution for 3 hours to get the free standing coatings. The free standing coatings were then oven dried for measuring the dry weight. The density of the free standing coatings is calculated by Archimedes' principle as given by Eq. 1.

$$\rho = \frac{w_1}{w_2 - w_3} \tag{1}$$

Where, ρ, w_1, w_2, and w_3 represent the density of the coating, initial dry weight of the coating, water saturated weight of the coating, and weight of coating in de-ionized water, respectively. The saturated weight of the coating was obtained by soaking the free standing coating in the

5

boiling water for one hour followed by measuring its weight using a precision weighing balance. The total porosity content can be evaluated from Eq. 2 as follows:

$$\text{Total porosity in the coating, } P_{total} = 1 - \left(\rho_{measured} \middle/ \rho_{theoretical} \right) \qquad (2)$$

The theoretical densities, $\rho_{theoretical}$, of YSZ, Al_2O_3, and CoNiCrAlY are 5.96 g/cm^3 [15], 3.98 g/cm^3 [15], and 7.24 g/cm^3[23], respectively. The theoretical densities of CoNiCrAlY-YSZ and YSZ-Al_2O_3 composite coatings were calculated using rule of mixture which are presented in Table II.

The coefficient of thermal expansion of the free standing as-sprayed coatings (with dimension of $10 \times 5 \times 1$ mm^3) was measured in air from 27 °C to 1000 °C using a dilatometer (NETZSCH DIL 402 C, Germany) at a heating rate of 10 K/min. Fractional change in length, $\Delta L/L$ as a function of temperature was measured and the coefficients of thermal expansion, α, was measured from the slope of the curve.

Thermal diffusivity of the freestanding coatings ($10 \times 10 \times 1$ mm^3) was measured using laser flash technique (LFA 427, Netschz, Germany) from 27 °C to 1000 °C under N_2 atmosphere. Both the surfaces of the coatings were coated with colloidal graphite for uniform absorption and emission of laser energy prior to laser flash test. The pulsed width is chosen to be 0.5 ms and the radiation model was used for calculation of thermal conductivity.

3.   Results & discussion

3.1.   Characterization of as-sprayed coating

6

Table 2 summarizes the density and porosity of the coatings measured by water displacement technique using Archimedes principle. Table 2 reveals that the density of the CoNiCrAlY/YSZ composite coating increases (and porosity content decreases) with the increase in CoNiCrAlY content in the coatings. The increase in density of the composite coating with increase in the CoNiCrAlY content is attributed to the proper bonding between the successive splats due to increased melting of the inflight metallic particles as compared to the only ceramic particles in the plasma jet. Gu et al [24] have also found similar trend on the variation of density with NiCrAlY content for the plasma sprayed ZrO_2:NiCrAlY composite coating. Generations of different type of porosities in thermal sprayed coating are believed to be due to improper melting of the powder particles, weak inter-splat bonding, etc. [25-28]. The presence of porosities has a significant role in reducing the thermal conductivity of the coatings. The shape and size of the porosities are the two important parameters which may affect the thermal conductivity more efficiently [29]. From Table 2, it is also evident that the density of the YSZ/Al_2O_3 composite coating decreases with increase in the Al_2O_3 content in the coating which may be attributed to the lower intrinsic density of the Al_2O_3 phase. In this regard, it is relevant to mention that though the open porosity content decreases with increase in the Al_2O_3 content, however, the variation of total porosity content with Al_2O_3 content do not follow any specific trend.

Fig. 3 shows the scanning electron micrographs of the cross-section of (a) 100% YSZ, (b) 70% YSZ + 30% CoNiCrAlY, (c) 50% YSZ + 50% CoNiCrAlY, (d) 30% YSZ + 70% CoNiCrAlY, and (e) 100% CoNiCrAlY coatings. The microstructures of the CoNiCrAlY/YSZ composite coatings show the presence of globular porosities, voids, intra-lamellar cracks/pores, and intra-lamellar cracks except for the 100% CoNiCrAlY coating. Fig. 3 (a) reveals the presence of various microstructural features (shown by arrowheads) in 100% YSZ. Due to the

7

100% ceramic nature of the coating, the inter-splat bonding is not so complete and hence, there are presence of fine inter-lamellar porosities. On the other hand, due to high melting point and low heat transfer characteristics of ceramic particles, few unmelted or resolidified particles are always present in the deposited coatings which contribute to the generation of different types porosities. From Figure 3 it is evident that the presence of inter-lamellar porosities is higher in 100% YSZ coating (100% ceramic) and decreases with increase in CoNiCrAlY content in the composite layer (Fig. 3(a) vis-à-vis Fig. 3(b-d)). Due to proper melting of CoNiCrAlY particles, an improved inter-splat bonding and decreased inter-lamellar porosities in the coating are observed. No visible micro-cracks and porosities are observed in 100% CoNiCrAlY coating (cf. Fig. 3(e)) due to its highest density among all other studied CoNiCrAlY/YSZ composite coatings (cf. Table 2). Oxide stringers are, however, observed in the 100% CoNiCrAlY coatings which is attributed to the oxidation of the powder particles during deposition process.

Fig. 4 shows the scanning electron micrographs of the cross-section of (a) 100% YSZ, (b) 70% YSZ + 30% Al_2O_3, (c) 50% YSZ + 50% Al_2O_3, (d) 30% YSZ + 70% Al_2O_3, and (e) 100% Al_2O_3 coatings developed on CoNiCrAlY bond coated INCONEL 718 substrate. A comparison between Fig. 3 and Fig. 4 reveals that in composite YSZ + Al_2O_3 coatings (Fig. 4(b-d)), there are presence of several types of microstructural defects such as inter-lamellar cracks/pores, intra-lamellar cracks, and globular porosities/voids which is mainly attributed to the nature of deposition process as well as the nature of feedstock powders for the deposition. Presences of several types of defects in the YSZ/Al_2O_3 composite coatings are almost similar as both the constituent phase involved in the composite coatings is ceramic in nature. However, absence of any trend in the porosity content (cf. Table 2) of the YSZ/Al_2O_3 composite coatings indicates that the difference in particle size and morphology of the YSZ and Al_2O_3 powder particles have

8

the dominant effect on the formation of porosities in the YSZ/Al_2O_3 composite coatings. These microstructural defects (porosities and micro cracks) are randomly distributed throughout the coating thickness. Improper melting of powder particles, entrapment of carrier gas, and weak inter-splat bonding are the primary causes for the formation of these microstructural defects [25-28]. Though these defects act as paths for the transport of oxygen, they also increase the strain tolerance capacity of the TBC and help in decreasing the thermal conductivity of a TBC [30]. Improper contacts between splats due to rapid solidification lead to formation of inter-lamellar cracks or porosities [31, 32]. The genesis of intra-lamellar cracks is from the quenching stress (tensile stress) relaxation of the individual splats during solidification of molten or semi-molten particles [31-33]. Intra-lamellar cracks have almost no effect on thermal conductivity reduction as they are aligned parallel to heat flux. However, these cracks help to maintain strain tolerance of the thermal barrier coatings in a thermal cycling environment [32, 33]. On the other hand, the inter-lamellar cracks/porosities, which scatters phonons, have the very dominant effect in reducing thermal conductivity as they are aligned perpendicular to the direction of heat flux [32, 34]. The inter-lamellar cracks/porosities, however, are the source of delamination in the thermal barrier coatings [30, 34].

Fig. 5 shows the scanning electron micrographs of the cross-section of fractured (a) 100% YSZ, (b) 70% YSZ + 30% CoNiCrAlY, (c) 50% YSZ + 50% CoNiCrAlY, (d) 30% YSZ + 70% CoNiCrAlY, and (e) 100% CoNiCrAlY coatings. Fractured cross-sections have been prepared by immersing the composite coatings in liquid nitrogen for 5 minutes followed by breaking it by bending. Fig. 5(a) it may be noted that there are presences of cleavage in the fractured surfaces and the coating consists of several layers with the width of individual layer to a thickness of 1.75 μm. In addition, the coating grows in columnar fashion with the width of individual column of

9

0.1 μm. From Figure 5(a) it may further be noted that there are presences of a few inter-columnar cracks in addition to the possibility of the presence of nano-pores in the inter-columnar interfaces. In addition, the layers are stacked uniformly over each other. There are also the presences of a few spherical porosities, possibly due to the entrapment of carrier gas during the solidification of the coating. From Fig. 5 it may be noted that the fractured surface of CoNiCrAlY coating shows no signature of brittle fracture, but, the tearing effect of the coating is visible from the microstructure. In addition, due to the ductile mature of the coating, the interface is curved in contrast to the straight interface observed in ceramic coating. The curved nature of the interface is attributed to the impact of the coating in molten/semi-molten state on the previously deposited surface at high velocity leading to deformation of the coating at the interface. There is presence of lamellar porosities at the interface between the splats and globular porosities present in a dis-continuous fashion possibly due to gas entrapment. CoNiCrAlY/YSZ composite coatings show the mixed mode failure with the presence of both brittle and ductile features. There is presence of cleavage surface in addition to deformation zone. Formation of many inter-lamellar porosities are evident from Fig. 5 (b-d) which is due to the generation of tensile stresses parallel to the splats interface or splat boundaries during bending. Hence, to conclude on the nature and variation of different types of microstructural defects with the composition of the CoNiCrAlY/YSZ composite coatings, low magnification scanning electron micrographs of the cross-section of the CoNiCrAlY/YSZ composite coatings are considered as presented in Fig. 3

Fig. 6 shows the scanning electron micrographs of the cross-section of fractured (a) 100% YSZ, (b) 70% YSZ + 30% Al_2O_3, (c) 50% YSZ + 50% Al_2O_3, (d) 30% YSZ + 70% Al_2O_3, and (e) 100% Al_2O_3 free standing coatings. From Fig.6 (a) and Fig. 6 (e), the average grain sizes of

YSZ and Al_2O_3 coatings, as measured by linear intercept method, are found to be ~140 nm and ~ 270 nm, respectively. The mechanism of thermal spray coating build up which is splat upon splat deposition is evident from Fig. 6. Formation of columnar grains and its directional growth is dependent on the direction of heat flow during solidification of splats which is towards the substrate. The presence of several types of microstructural defects (globular pores, inter-lamellar and intra-lamellar pores) is shown in Fig. 6. Formation of these microstructural defects in the microstructure of plasma sprayed coating may be due to the following reasons: (a) incomplete filling of irregular or rough surface which is generated due to the incomplete melting or re-solidification of powder particles and/or solidification of detached droplets from the impacting droplets, (ii) due to the entrapment of gas within the splat and (iii) due to the presence of residual stress in the splats [25-28]. As discussed earlier, improper contacts between splats resulting due to rapid solidification of molten particles leads to formation of inter-lamellar cracks/porosities [31, 32]. Tensile quenching stress relaxation during rapid solidification of individual splat is the source of the intra-lamellar cracks [31-33].

Fig. 7 shows the X-ray diffraction profiles of 100% YSZ coating (plot 1), 70% YSZ + 30% CoNiCrAlY coating (plot 2), 50% YSZ + 50% CoNiCrAlY coating (plot 3), and 30% YSZ + 70% CoNiCrAlY coating (plot 4). Presence of non-transformable tetragonal zirconia (t′-ZrO_2) is evident in the 100% YSZ coating (plot 1). No evidence of any phase other than t′-ZrO_2 is found in the 100% YSZ coating. The formation of non-transformable zirconia phase in the 100% YSZ coating is due to the very high cooling rate achieved during solidification of YSZ splats during plasma spray deposition. On the other hand, the composite coatings of YSZ and CoNiCrAlY (with the ratio of 70:30, 50:50, and 30:70) show the presence of γ-Co phase (matrix) along with t′-ZrO_2 phase in the X-ray diffraction profiles of the composite coatings. The

11

evidence of γ-Co phase in the X-ray diffraction profiles of the coatings is supported by the presence of γ-Co phase in the composite coatings. It has been reported that the plasma spraying of metallic alloy powders results in the formation of different oxides in the coating according the composition of the alloy powder [35, 36]. However, there is no evidence of any oxides in the X-ray diffraction profiles of the composite coatings which could be due to the very small volume fraction of the oxides. There is also no evidence of β-CoAl phase which forms around $2\theta \approx 44.8°$ [35] in the X-ray diffraction profiles of the composite coatings which could be due to the very small volume fraction of β-CoAl phase. β-CoAl phase is important as it acts as an aluminum reservoir in the CoNiCrAlY coating which supplies aluminum to form/maintain a stable alumina layer during elevated temperature exposure [35, 36].

Fig. 8 shows the X-ray diffraction profiles of the 100% YSZ coating (plot 1), 70% YSZ + 30% Al_2O_3 coating (plot 2), 50% YSZ + 50% Al_2O_3 coating (plot 3), 30% YSZ + 70% Al_2O_3 coating (plot 4), and 100% Al_2O_3 coating (plot 5). The 100% YSZ coating contains the t′-ZrO_2 phase which has already been discussed in the previous paragraph. The XRD profiles of the YSZ and Al_2O_3 composite coatings show presence of γ-Al_2O_3 as the major phase with few α-Al_2O_3 phases. Comparing the XRD profiles of the composite coatings containing Al_2O_3 with the XRD scan of Al_2O_3 powder (cf. Fig. 1 (b)), it may be observed that the α-Al_2O_3 phase present in Al_2O_3 powder has now been transferred to γ-Al_2O_3 after plasma spraying with the presence of few α-Al_2O_3 phases. Retention of high temperature γ-Al_2O_3 phase in the plasma sprayed composite coating of YSZ and Al_2O_3 is attributed to the melting of powder particles followed by rapid solidification of splats during plasma spray deposition which is consistent with the other reported investigations [22, 37]. Retention of very few α-Al_2O_3 phases in the composite coatings is due to the incomplete or partial melting of the powder particles during plasma spraying. From Fig. 8, it

12

may be noted that the intensities of the γ-Al_2O_3 phase and the t$'$-ZrO_2 phases vary with the composition of the composite coatings.

3.2. Coefficient of thermal expansion of composite coatings

Coefficient of thermal expansion (CTE) of a material gives a prior impression about its service life when exposed to an elevated temperature environment. A prior knowledge of CTE of the materials would subsequently, assist to design the component to enhance its service life. Fig. 9 shows the variation of thermal expansion per unit length ($\Delta L/L$) with temperature for CoNiCrAlY/YSZ composite coatings between 27 °C to 1000 °C. Thermal expansion in all composite coatings increases with increase in the temperature. At low temperature regime (< 600 °C), the difference in thermal expansion between the metallic based and ceramic based coating is low; however, beyond 600 °C the difference in thermal expansion increases. The change in nature of the plot at high temperature may be attributed to the change in microstructure and, or phase during heating [38]. The slope of the curve for 100% CoNiCrAlY coating shows change in the temperature range of 27 °C - 600 °C, 600 °C - 800 °C, and 800 °C - 1000 °C, respectively. Similarly, the curve for 70% CoNiCrAlY + 30% YSZ and 50% CoNiCrAlY + 50% YSZ coatings show change in slope between 27 °C - 500 °C, 500 °C - 750 °C, and 750 °C - 1000 °C, respectively. However, no significant change in the slope of the curve is observed for 30% CoNiCrAlY + 70% YSZ and 100% YSZ coatings.

From the slope of thermal expansion curve (cf. Fig. 9), the coefficient of thermal expansion (α) has been measured under different temperature range and then averaged over the complete temperature range to evaluate α_{avg} of the coatings from 27 °C to 1000 °C. For 100% CoNiCrAlY coating, α in the temperature range of 27 °C - 600 °C, 600 °C - 800 °C, and 800 °C -

13

1000 °C are measured to be 18.4×10^{-6}/°C, 22.4×10^{-6}/°C, and 24.4×10^{-6}/°C, respectively. For 70% CoNiCrAlY + 30% YSZ coating, α in the temperature range of 27 °C - 500 °C, 500 °C - 750 °C, and 750 °C - 1000 °C are measured to be 17.3×10^{-6}/°C, 19.04×10^{-6}/°C, and 19.9×10^{-6}/°C, respectively. For 50% CoNiCrAlY + 50% YSZ coating, α in the temperature range of 27 °C - 500 °C, 500 °C - 750 °C, and 750 °C - 1000 °C are measured to be 15.9×10^{-6}/°C, 17.8×10^{-6}/°C, and 16.8×10^{-6}/°C, respectively. As no significance change in slope of the curve is observed for 30% CoNiCrAlY + 70% YSZ and 100% YSZ coatings, the α value has been calculated directly from the temperature range of 27 °C to 1000 °C. The average values of α from 27 °C to 1000 °C are presented in Table 3. The $α_{avg}$ for 100% YSZ, 70% YSZ + 30% CoNiCrAlY, 50% YSZ + 50% CoNiCrAlY, 30% YSZ + 70% CoNiCrAlY, and 100% CoNiCrAlY composite coatings are found to be 13.1×10^{-6}/°C, 14.9×10^{-6}/°C, 16.8×10^{-6}/°C, 18.3×10^{-6}/°C, and 21.2×10^{-6}/°C, respectively. The coefficient of thermal expansion increases with the increase in the volume fraction of CoNiCrAlY in the composite coating as metals tend to expand more than ceramics. The gradual variation in coefficient of thermal expansion of the composite coatings with the gradual change in the composition of composite coatings may be useful in designing a functionally graded TBC.

Fig. 10 shows the variation of thermal expansion per unit length (ΔL/L) with temperature for YSZ/Al$_2$O$_3$ composite coatings from 27 °C to 1000 °C. Fig. 10 illustrates that ΔL/L increases with increase in the temperature for YSZ/Al$_2$O$_3$ composite coatings. The average values of $α_{avg}$ within the temperature range of 27 °C to 1000 °C for different plasma sprayed composite coatings are presented in Table 4. The coefficient of thermal expansion is measured to be 13.1×10^{-6}/°C for 100% YSZ coating, 11.9×10^{-6}/°C for 70% YSZ + 30% Al$_2$O$_3$ composite coating, 11×10^{-6}/°C for 50% YSZ + 50% Al$_2$O$_3$ composite coating, 10.7×10^{-6}/°C for 30% YSZ + 70%

14

Al$_2$O$_3$ composite coating, and 9.5×10^{-6} /°C for 100% Al$_2$O$_3$ coating. Table 4 reveals that the coefficient of thermal expansion of the YSZ/Al$_2$O$_3$ composite coatings increases with the increase in the volume fraction of YSZ in the composite coatings. The gradual variation in coefficient of thermal expansion would help to minimize the thermal stress developed due to thermal expansion mismatch in thermal barrier coating system.

3.3. Thermal diffusivity analysis of the composite coatings

Fig. 11 shows the variation of thermal diffusivity as a function of temperature for 100% YSZ, 70% YSZ + 30% CoNiCrAlY, 50% YSZ + 50% CoNiCrAlY, 30% YSZ + 70% CoNiCrAlY, and 70% YSZ + 30% CoNiCrAlY, and 100% CoNiCrAlY composite coatings. From Fig. 11, it may be noted that 100% YSZ coating shows decrease in thermal diffusivity with increase in the temperature suggesting phonon conduction mechanism of heat flow as dominant mechanism. The thermal diffusivity of 100% YSZ coating decreases with temperature (0.37 mm^2/s and 0.206 mm^2/s at room temperature and at 1000 °C, respectively). On the other hand, the CoNiCrAlY/YSZ composite coatings show an initial decrease in thermal diffusivity up to 400 °C following which it increases monotonically with temperature up to 1000 °C. From Fig. 11, it may also be noted that the increase in the value of thermal diffusivity beyond 400 °C is prominent with the increased presence of CoNiCrAlY phase in the composite coatings. The thermal diffusivities for 70% YSZ + 30% CoNiCrAlY, 50% YSZ + 50% CoNiCrAlY, 30% YSZ + 70% CoNiCrAlY, and 100% CoNiCrAlY composite coatings, at room temperature, are measured to be 0.836 mm^2/s, 1.015 mm^2/s, 1.167 mm^2/s, and 1.1331 mm^2/s, respectively which increases to 1.171 mm^2/s, 1.253 mm^2/s, 1.51 mm^2/s, and 1.896 mm^2/s at 1000 °C. The increase in the thermal diffusivity values of the composite coatings at higher temperature has been

15

reported due to increased inter-splat contact because of grain growth at elevated temperature [7, 39].

Fig. 12 shows the variation of thermal diffusivity as a function of temperature for 100% YSZ, 70% YSZ + 30% Al_2O_3, 50% YSZ + 50% Al_2O_3, 30% YSZ + 70% Al_2O_3, and 100% Al_2O_3 coatings developed by plasma spraying. From Fig. 12, it may be noted that the thermal diffusivity decreases monotonically with the increase in temperature from room temperature to 1000 °C for all YSZ/Al_2O_3 composite coatings. The room temperature thermal diffusivity in 100% Al_2O_3 coating is 1.51 mm^2/s which decreases to 0.5 mm^2/s at 1000 °C. The thermal diffusivities of 70% Al_2O_3 + 30% YSZ, 50% Al_2O_3 + 50% YSZ, 30% Al_2O_3 + 70% YSZ, and 100% YSZ coatings, at room temperature, are measured to be 0.808 mm^2/s, 0.581 mm^2/s, 0.556 mm^2/s, and 0.37 mm^2/s, respectively which decreases to 0.275 mm^2/s, 0.246 mm^2/s, 0.24 mm^2/s, and 0.206 mm^2/s at 1000 °C, respectively. The dependence of thermal diffusivity inversely with temperature in these coatings suggest that the mechanism of heat transfer is, predominantly, by phonon conduction which is mostly observed in polycrystalline insulating materials [40].

3.4. Specific Heat Capacity

Specific heat capacity of the 100% YSZ, 100% CoNiCrAlY, and 100% Al_2O_3 coatings have been taken from literature which is presented in Table 5 [41-43]. From these literature values the specific heat capacities of CoNiCrAlY/YSZ composite coatings and YSZ/Al_2O_3 composite coatings have been determined by rule of mixture and are summarized in Table 5.

3.5. Thermal conductivity analysis

In an insulating crystalline solid, the thermal conduction is mainly governed by lattice vibrations (phonons) and radiations (photons). The contribution from photons is dominant at high temperature (>1200 °C for zirconia [44]). The thermal conductivity of an insulating material is proportional to the mean free path of phonons according to the following relation [45]:

$$k = \left(\frac{1}{3} C_v v \right) l \qquad (3)$$

Where, c_v is the specific heat capacity, v is the phonon velocity, and l is the mean free path of phonons. Eq. 3 reveals that it is possible to reduce the intrinsic thermal conductivity of a material by lowering the mean free path of the phonons, lowering the phonon velocity, and lowering the specific heat capacity. In practice, the intrinsic thermal conductivity of an insulating solid may be lowered by incorporating lattice imperfections (dislocations, vacancies, grain boundaries, size of solute atoms and phonons) which helps in scattering the moving phonons, and thereby decreasing in the mean free path (l) of phonons [46]. The dependence of mean free path (l) on the lattice imperfections is defined by

$$\frac{1}{l} = \frac{1}{l_i} + \frac{1}{l_{vac}} + \frac{1}{l_{gb}} + \frac{1}{l_{strain}} \qquad (4)$$

Where, l_i, l_{vac}, l_{gb}, and l_{strain} are the contributions from phonon mean free paths from intrinsic conductivity of the material, like point defects or vacancies, grain boundaries, and strain field formed due to size difference between solute atoms and the matrix. The thermal conductivity of a material is the multiplication product of thermal diffusivity (λ) of the material, density (ρ) and specific heat of that material (c_p) according to the following relation [47].

$$k = \lambda \times \rho \times c_p \qquad\qquad (5)$$

3.5.1. Experimental Data

Fig. 13 shows the variation of thermal conductivity of CoNiCrAlY/YSZ composite coatings with temperature. Fig. 13 illustrates slow decrease in the value of thermal conductivity with increase in temperature for 100% YSZ coating suggesting the phonon conduction as the dominant mechanism of heat conduction. For a perfect solid material without the presence of any defects, the thermal conductivity due to phonon conduction can be expressed by:

$$k_p \propto \frac{1}{T} \qquad\qquad (6)$$

Where, T is the temperature on absolute scale.

The value of thermal conductivity for 100% YSZ coating, at 27 °C, is found to be 0.869 W.m^{-1}.K^{-1} which decreases to 0.667 W.m^{-1}K^{-1} at 1000°C. On the other hand, for CoNiCrAlY/YSZ composite coatings, the thermal conductivity remains almost stable from 27 °C to 400 °C and beyond 400 °C, the thermal conductivity increases monotonically up to 1000 °C. The thermal conductivities for 70% YSZ + 30% CoNiCrAlY, 50% YSZ + 50% CoNiCrAlY, 30% YSZ + 50% CoNiCrAlY, and 100% CoNiCrAlY coatings, at 27 °C, are 2.282 W.m^{-1}.K^{-1}, 3.091 W.m^{-1}.K^{-1}, 3.805 W.m^{-1}.K^{-1}, and 4.685 W.m^{-1}.K^{-1}, respectively. The corresponding thermal conductivity values increases to 4.446 W.m^{-1}.K^{-1}, 5.335 W.m^{-1}.K^{-1}, 6.928 W.m^{-1}.K^{-1}, and 9.477 W.m^{-1}.K^{-1}, respectively at 1000 °C. As electron conduction mechanism is dominant at low temperature, the increase in thermal conductivity value at high temperature may be attributed to the densification of coating due to grain growth [7, 39].

Fig. 14 shows the variation of thermal conductivity of YSZ, Al$_2$O$_3$, and YSZ/Al$_2$O$_3$ composite coatings with temperature. From Fig. 14, it is evident that the thermal conductivity of

18

all the composite coatings shows an inverse dependence on temperature suggesting that the phonon-phonon scattering as dominant mechanism of increased thermal resistance with the increase in temperature. While at room temperature 100% Al_2O_3, 70% Al_2O_3 + 30% YSZ, 50% Al_2O_3 + 50% YSZ, 30% Al_2O_3 + 70% YSZ, and 100% YSZ coatings have thermal conductivities of 3.973 $W.m^{-1}.K^{-1}$, 1.983 $W.m^{-1}.K^{-1}$, 1.439 $W.m^{-1}.K^{-1}$, 1.337 $W.m^{-1}.K^{-1}$, and 0.87 $W.m^{-1}.K^{-1}$, respectively, it decreases to 2.154 $W.m^{-1}.K^{-1}$, 1.068 $W.m^{-1}.K^{-1}$, 0.936 $W.m^{-1}.K^{-1}$, 0.856 $W.m^{-1}.K^{-1}$, and 0.666 $W.m^{-1}.K^{-1}$, respectively, at 1000 °C, due to increased phonon-phonon scattering at elevated temperature.

3.5.2. Theoretical Prediction

In polycrystalline materials, the thermal conductivity of a material varies with the grain size according to the following relation [48]:

$$\frac{1}{k_{poly}} = \left(\frac{1}{k_{singlecrystal}} \right) + n \times R_{gb} \tag{7}$$

Where, k_{poly} is the thermal conductivity of dense polycrystalline material, $k_{single\ crystal}$ is the thermal conductivity of single crystal, n (1/grain size) is the number of grains per unit length, and R_{gb} is the grain boundary thermal resistance. The grain sizes in YSZ and Al_2O_3 coatings are 140 nm and 270 nm, respectively as measured by linear intercept method.

For 100% YSZ, k for a single crystal is 2.2 W m^{-1} K^{-1} [45], n is 7142857 m^{-1} and R_{gb} is 4.5×10^{-9} m^2 K/W [49]. So, k_{poly} is 2.08 W m^{-1} K^{-1} for YSZ. Similarly, for 100% Al_2O_3, $k_{single\ crystal}$ is 30 W m^{-1} K^{-1}[49], n is 3703703 m^{-1} and R_{gb} is 1.3×10^{-8} m^2 K/W [50]. So, k_{poly} is 12.35 W m^{-1} K^{-1} for Al_2O_3.

19

The thermal conductivities of fully dense YSZ and Al_2O_3 coatings are calculated by Eq. 7. The thermal conductivities of fully dense YSZ/Al_2O_3 composite coatings with different powder mixture have been calculated by rule of mixture from the 100% dense values of YSZ and Al_2O_3 coatings. As there are number of alloying elements present in CoNiCrAlY alloy, the thermal conductivity of dense CoNiCrAlY alloy have been calculated using Klemens' equation [51]. Thermal conductivities of fully dense CoNiCrAlY/YSZ composites with different mixing ratio of CoNiCrAlY and YSZ powders have been calculated by rule of mixture. All the calculations have been made in volume percentage.

Fig. 15 shows the variation of the measured thermal conductivity and theoretical thermal conductivity (according to Eq. 7) with CoNiCrAlY mixing ratio (vol.%) in the CoNiCrAlY/YSZ composite coatings. From Fig. 15, it is evident that the measured thermal conductivity of composite coatings increases with the increase in the volume fraction of CoNiCrAlY phase. The observation is attributed the (a) high intrinsic thermal conductivity of metallic CoNiCrAlY phase than YSZ phase and (b) decrease in volume fraction of porosity with increase in metallic CoNiCrAlY volume fraction in the composite coatings. Comparing the experimentally measured thermal conductivity values and theoretically obtained (using Eq. 7) values of CoNiCrAlY/YSZ composite coatings, it is evident that there exist a clear difference between the measured values and theoretical values. The measured thermal conductivity is lower than the theoretical thermal conductivity. Presences of porosities are accounted for the observed difference in the thermal conductivities according to Eq. 8. From Fig. 15, it may also be noted that with increase in volume fraction of CoNiCrAlY phase, the difference in experimental thermal conductivity and theoretical thermal conductivity decreases from 58% for 100% YSZ coatings to 4% for 100% CoNiCrAlY coatings. This observation is supported by the fact that decrease in the volume

20

fraction porosities is observed with increase in the volume fraction of CoNiCrAlY phase in the composite coatings (cf. Table 2).

$$k_{eff} = k_{intrinsic} \text{ (Grain size)} + \text{Porosity (Volume fraction, Morphology)} + \text{Inter-splat thermal resistance}$$

(8)

Where, k_{eff} is the effective thermal conductivity of the thermal spray coating which is a function of intrinsic thermal conductivity ($k_{intrinsic}$), porosity, and inter-splat thermal resistance.

Fig. 16 shows the variation of the measured thermal conductivity and theoretical thermal conductivity (according to Eq. 7) with Al_2O_3 mixing ratio in the YSZ/Al_2O_3 composite coatings. A large difference in the values of measured thermal conductivity and theoretical conductivity is observed as presented in Fig. 16. With increase in the volume fraction of Al_2O_3 phase in the YSZ/Al_2O_3 composite coatings, the difference in experimental thermal conductivity and theoretical thermal conductivity increases from 58% for 100% YSZ coatings to 68% for 100% Al_2O_3 coatings. Comparing Fig. 15 and Fig. 16, it may be noted that the difference in the measured and theoretical thermal conductivities is larger for the Al_2O_3/YSZ composite coatings than for the CoNiCrAlY/YSZ composite coatings. Presence of large volume fraction of porosities is the reason behind the observed difference according to Eq. 8. However, presence of porosities/microcracks aligned perpendicular to the direction of heat flow is the reason behind the large reduction in the thermal conductivity of the YSZ/Al_2O_3 composite coatings. To understand the effect of microstructural defects (morphology of porosities) on the thermal conductivity of the composite coatings, different analytical models have been used and subsequently discussed in the next section.

3.5.3. Analytical Predictions

21

Analytical models are useful tools to predict the dependence of thermal conductivity with porosity and hence, to design the microstructure with optimum porosity level [16-18, 20-22]. Presence of porosities in the microstructure of plasma sprayed coating reduces the thermal conductivity significantly. Several analytical models have been developed to predict the effective thermal conductivity of a two phase material where solid matrix is taken as one phase and the porosity as another phase [20-22]. Effective thermal conductivity, k_{eff} of a two phase material can be expressed by different analytical models as

Landauer model [20]

$$k_{eff} = \frac{1}{4}\left[k_p(3V_p - 1) + k_m(2 - 3V_p) + \sqrt{[k_p(3V_p - 1) + k_m(2 - 3V_p)]^2 + 8k_p \times k_m} \right] \qquad (9)$$

Where, k_p (= 0.026 W.m^{-1}.K^{-1}) refers to the thermal conductivity of the pore. The model assumes completely random distribution of two phases and it does not depend on the shape of pores.

Meredith and Tobias model [21]

$$k_{eff} = k_m\left[\frac{(2 - V_p)}{2 + (W-1)V_P} \right]\left[\frac{2(1 - V_p)}{2(1 - V_P) + WV_P} \right] \qquad (10)$$

Where, $W = \frac{1}{3}\left[\left(\frac{1}{2F}\right) + \left(\frac{2}{(1-F)}\right)\right]$, F is the shape factor for randomly oriented pores.

For lamellar porosity, F = 0.083 and for spherical porosity, F = 0.333 [16].

Ravichandran model [22]

$$k_{eff} = k_m\left(1 - V_p^{\frac{2}{3}}\right) \qquad (11)$$

Ravichandran [22] model includes the effect of thermal resistance offered by the splat-splat interface on the effective thermal conductivity apart from porosity content.

Maxwell model [16]

22

$$k_{eff} = k_m \left[1 - \left(\frac{3}{2} \right) V_P \right] \tag{12}$$

Maxwell model assumes a very dilute distribution of non-interacting spherical porosities (< 10%).

Bruggeman model [16]

$$k_{eff} = k_m (1 - V_P)^X \tag{13}$$

The factor $X = \left[\frac{(1 - \cos^2 \beta)}{1 - F} \right] + \left[\frac{\cos^2 \beta}{2F} \right]$

Where, F is the shape factor for the porosities and β is the angle between the revolution axis and heat flux. For lamellar porosity, X = 6 as F = 0.083 and $\beta = 0°$ and for spherical porosity, X = 1.5 as F = 0.333 and $\beta = 0°$ or $90°$ [16].

In all equations, k_m refers to the thermal conductivity of matrix and V_p is the volume fraction of pores. Thermal conductivity of the matrix implies the theoretical thermal conductivity of dense composite coatings calculated by Eq. 7. Effective thermal conductivity of the CoNiCrAlY/YSZ and YSZ/Al$_2$O$_3$ composite coatings have been calculated using Eq. 9 to Eq. 13 taking porosity into account which is plotted in Fig. 17 and Fig. 18. All the theoretical values of thermal conductivities are calculated at room temperature as the porosity of the coatings have been calculated at room temperature.

Fig. 17 shows the variation of effective thermal conductivity of the CoNiCrAlY/YSZ composite coatings, measured experimentally as well as theoretically using different analytical models, at room temperature with different CoNiCrAlY mixing ratio in the CoNiCrAlY/YSZ composite coatings. From Fig. 17, it may be noted that the experimental results show a good match with few analytical models. The 100% YSZ coating shows a good match with the Bruggeman model with X = 6 (for lamellar porosities). The microstructure of 100% YSZ

23

contains more amounts of oblate shaped defects due to unmelted and resolidified particles (cf. Fig. 3a). However, the experimental value of effective thermal conductivity in 70% YSZ + 30% CoNiCrAlY and 50% YSZ + 50% CoNiCrAlY coatings match to the Ravichandran model which may be attributed to the effect of thermal resistance offered by the interface between splats. Apart from the usual microstructural defects (porosities and microcracks), the improper contacts between the successive splats (cf. Fig. 3) are also responsible for lowering the effective thermal conductivity as these do not act as continuous path for phonon and electron motion or the phonons and electrons get scattered at the splat boundaries. With further increase in the CoNiCrAlY content in composite coating (i.e. 30% YSZ + 70% CoNiCrAlY and 100% CoNiCrAlY coatings), the experimentally obtained effective thermal conductivity matches to the Maxwell model and Bruggeman model (X=1.5). Maxwell model assumes dilute dispersion of spherical pores. From Table 2, it may be noted that the 30% YSZ + 70% CoNiCrAlY and 100% CoNiCrAlY coatings possess porosity contents of 3.2 % and 2.8 %, respectively, which matches to the assumption of low porosity as assumed in Maxwell model. Also, it is understood that the melting of metallic particles in the plasma leads to a high degree flattening or spreading as compared to ceramic particles. Higher degree of flattening or spreading of the melted particles lead to decrease in the content of inter-lamellar porosity, whereas the gas entrapment within the particles or deposition of unmelted or resolidified particles lead to formation of spherical porosities which is well complemented by the Maxwell model and Bruggeman model (X = 1.5).

Effective thermal conductivities of the YSZ/Al_2O_3 composite coatings have been calculated by Eq. 9 to Eq. 13 and compared with the experimentally measured thermal conductivities of the composite coatings at room temperature. Fig. 18 shows the variation of effective thermal conductivities of the YSZ/Al_2O_3 composite coatings, measured experimentally

24

as well as through different analytical models, with the Al_2O_3 mixing ratio in the YSZ/Al_2O_3 composite coatings at room temperature. From Fig. 18, it is clear that the Bruggeman model with $X = 6$ (i.e. for lamellar porosity) closely matches with the experimentally observed values for all YSZ/Al_2O_3 composite coatings which suggest that the inter-lamellar porosities are the dominant microstructural defects in lowering the thermal conductivity of YSZ/Al_2O_3 composite coatings. Plasma sprayed coatings, generally, have two different types of porosity (lamellar porosity and globular) which reduces the overall thermal conductivity. Lamellar porosities which are aligned perpendicular to the direction of heat flow lower the thermal conductivity, efficiently. The matching of Brugemann model with the experimentally measured value is attributed to the presence of a large area fraction of inter-lamellar porosities in the microstructure of YSZ/Al_2O_3 coating (cf. Fig. 4). The formation of inter-lamellar porosities in ceramic coating is attributed to the deposition of unmelted or resolidified particles as well as due to poor bonding between successive splats as ceramic particles has high melting point and low thermal conductivity.

From Fig. 17 and Fig. 18, it can be noted that for 100% ceramic coatings, Bruggeman model is showing an excellent match with the experimental data for X value of 6. While for the composite coatings with metallic contents up to 50%, Ravichandran Model is showing good match with the experimental results. With further increase in metallic contents, the Bruggeman model with $X = 1.5$ and Maxwell model are showing good match. This observation suggests that for ceramic YSZ/Al_2O_3 composite coatings, lamellar porosities are playing main role in reducing the overall thermal conductivity of the coating, whereas for CoNiCrAlY/YSZ composite coating with higher volume fraction of CoNiCrAlY ($> 50\%$), the spherical porosities are dominant.

4. Conclusions

In the present study, thermal properties of the CoNiCrAlY/YSZ and Al_2O_3/YSZ composite coatings have been investigated and the mechanism of the reduction in thermal conductivity has been correlated with the defect morphology vis-à-vis the composition. From the detailed investigations, the following conclusions may be drawn:

1. Several types of microstructural defects (inter-lamellar porosities, intra-lamellar cracks, globular porosities) were observed in the microstructure of CoNiCrAlY/YSZ and YSZ/Al_2O_3 composite coatings.

2. The volume fractions of porosities in the CoNiCrAlY/YSZ composite coatings were found to decrease with the increase in the CoNiCrAlY content in the composite coatings. No trend in the volume fraction of porosity with the composition of the YSZ/Al_2O_3 composite coatings was observed.

3. A compositional dependent change in the coefficient of thermal expansion was observed for the CoNiCrAlY/YSZ and YSZ/Al_2O_3 composite coatings. At low temperature regime (< 600 °C), the difference in thermal expansion between the CoNiCrAlY/YSZ composite coatings was less which started increasing beyond 600 °C.

4. Thermal diffusivity and thermal conductivity also showed gradual change in its value with change in composition of composite coatings in CoNiCrAlY/YSZ and YSZ/Al_2O_3 composite coatings. The thermal conductivity was initially remain stable up to 400 °C beyond which it increased monotonically for all composition of CoNiCrAlY/YSZ composite coatings except for 100% YSZ coating.

5. A comparison between the measured thermal conductivity and the theoretical conductivity of the CoNiCrAlY/YSZ and YSZ/Al_2O_3 composite coatings showed that the presence of

porosities and its morphology has a strong effect in reducing the thermal conductivity of the composite coatings.

6. Model based analysis was found to be helpful in predicting the compositional dependent morphology of porosities in CoNiCrAlY/YSZ and YSZ/Al$_2$O$_3$ composite coatings. The presence of inter-lamellar porosities was responsible for reducing the thermal conductivity of ceramic composite coatings. However, presence of CoNiCrAlY metallic phase into the composite coatings changed the mechanism of thermal conductivity reduction to spherical porosities.

References

[1] A. Feuerstein, J. Knapp, T. Taylor, A. Ashary, A. Bolcavage, N. Hitchman, Technical and economical aspects of current thermal barrier coating systems for gas turbine engines by thermal spray and EBPVD: A review, J. Therm. Spray Technol. 17 (2008) 199-213.

[2] S. Bose, J. DeMasi-Marcin, Thermal barrier coating experience in gas turbine engines at Pratt & Whitney, J. Therm. Spray Technol. 6 (1997) 99-104.

[3] B.A. Pint, I.G. Wright, W.J. Brindley, Evaluation of thermal barrier coating systems on novel substrates, J. Therm. Spray Technol. 9 (2000) 198-203.

27

[4] W.Y. Lee, D.P. Stinton, C.C. Berndt, F. Erdogan, Y.D. Lee, Z. Mutasim, Concept of functionally graded materials for advanced thermal barrier coating applications: A review, J. Am. Ceram. Soc. 79 (1996) 3003-3012.

[5] A. Kawasaki R. Watanabe, Thermal fracture behavior of metal/ceramic functionally graded materials, Eng. Fract. Mech. 69 (2002) 1713-1728.

[6] K.A. Khor Y.W. Zu, Effects of residual stress on the performance of plasma sprayed functionally graded ZrO_2:NiCoCrAlY coatings, Mater. Sci. Eng. A 277 (2000) 64-76.

[7] K.A. Khor, Z.L. Dong, Y.W. Zu, Plasma sprayed functionally graded thermal barrier coatings, Mater. Lett. 38 (1999) 437-444.

[8] K.A. Khor, Y.W. Zu, Thermal properties of plasma-sprayed functionally graded thermal barrier coatings, Thin Solid Films 372 (2000) 104-113.

[9] K.A. Khor, Z.L. Dong, Y.W. Zu, Influence of oxide mixtures on mechanical properties of plasma sprayed functionally graded coating, Thin Solid Films 368 (2000) 86-92.

[10] Z.L. Dong, K.A. Khor, Y.W. Zu, Microstructure formation in plasma-sprayed functionally graded NiCoCrAlY/Yttria-stabilized zirconia coatings, Surf. Coat. Technol. 114 (1999) 181-86.

[11] G. Sreedhar, V.S. Raja, Hot corrosion of YSZ/Al_2O_3 dispersed NiCrAlY plasma-sprayed coatings in Na_2SO_4–10 wt.% NaCl melt, Corros. Sci.52 (2010) 2592–2602.

[12] G. Shanmugavelayutham, A. Kobayashi, Mechanical properties and oxidation behaviour of plasma sprayed functionally graded zirconia–alumina thermal barrier coatings, Mater. Chem. Phys. 103 (2007) 283-289.

[13] X. Chen, Y. Zhao, L. Gua, B. Zoua, Y. Wang, X. Cao, Hot corrosion behaviour of plasma sprayed YSZ/LaMgAl11O19 composite coatings in molten sulfate–vanadate salt, Corros. Sci. 53 (2011) 2335–2343.

[14] A.M. Limarga, S. Widjaja, T.H. Yip, Mechanical properties and oxidation resistance of plasma-sprayed multilayered Al_2O_3/ZrO_2 thermal barrier coatings, Surf. Coat. Technol. 197 (2005) 93–102.

[15] F. Yang, X. Zhao, P. Xiao, Thermal conductivities of YSZ/Al_2O_3 composites, J. Eur. Ceram. Soc. 30 (2010) 3111–3116.

[16] F. Cernuschi, S. Ahmaniemi, P. Vuoristo, T. Mantyla, Modelling of thermal conductivity of porous materials: application to thick thermal barrier coating, J. Eur. Ceram. Soc. 24 (2004) 2657–2667.

[17] A.D. Jadhav, N.P. Padture, E.H. Jordan, M. Gell, P. Miranzo, E.R. Fuller Jr., Low-thermal-conductivity plasma-sprayed thermal barrier coatings with engineered microstructures, Acta Mater. 54 (2006) 3343–3349.

[18] S.R. Bakshi, K. Balani, A. Agarwal, Thermal conductivity of plasma-sprayed aluminum oxide—multiwalled carbon nanotube composites, J. Am. Ceram. Soc. 91 (2008) 942–947.

[19] Y. Wang, W. Wu, X. Zheng, Y. Zeng, M. Ding, and C. Zhang, Relationship between the microstructure and thermal conductivity of plasma-sprayed ZrO_2 coatings, J. Therm. Spray Technol. 20 (2011)1177-1182.

[20] R. Landauer, The electrical resistance of binary metallic mixtures, J. Appl. Phys. 21 (1952) 779–784.

[21] R.E. Meredith, C.W. Tobias, Conduction in heterogeneous systems, in: C.W. Tobias (ed.), Advances in electrochemistry and electrochemical engineering, Interscience, New York, 1962, pp. 15-47.

[22] K.S. Ravichandran, K. An, R.E. Dutton, S.L. Semiatin, Thermal conductivity of plasma-sprayed monolithic and multilayer coatings of alumina and yttria-stabilized zirconia, J. Am. Ceram. Soc. 82 (1999) 673–682.

[23] S. Todde, R. Licheri, R. Orrù, G Cao, Spark plasma sintering processing for the evaluation of cryomilled CoNiCrAlY alloys for high temperature applications in oxidizing environment, Chem Eng J. 200/202 (2012) 68–80.

[24] Y.W. Gu, K.A. Khor, Y.Q. Fu, Y. Wang Functionally graded ZrOz-NiCrA1Y coatings prepared by plasma spraying using pre-mixed, spheroidized powders, Surf. Coat. Technol. 96 (I997) 305-312.

[25] J. Ilavsky, A.J. Allen, G.G. Long, S. Krueger, Influence of spray angle on the pore and crack microstructure of plasma-sprayed deposits, J. Am. Ceram. Soc. 80 (1997) 733–742.

[26] S.H. Leigh, C.C. Berndt, Quantitative evaluation of void distributions within a plasma-sprayed ceramic, J. Am. Ceram. Soc. 82 (1999) 17–21.

[27] M. Xue, S. Chandra, J. Mostaghimi, H.R. Salimijazi, Formation of pores in thermal spray coatings due to incomplete filling of crevices in patterned surfaces, Plasma Chem. Plasma Process 27 (2007) 647–657.

[28] J.A. Gan, C.C. Berndt, Effects of standoff distance on porosity, phase distribution and mechanical properties of plasma sprayed Nd–Fe–B coatings, Surf. Coat. Technol. 216 (2013) 127–138.

[29] P. Carpio, Q. Blochet, B. Pateyron, L. Pawłowski, M. Dolores Salvador, A. Borrell, E. Sánchez, Correlation of thermal conductivity of suspension plasma sprayed yttria stabilized zirconia coatings with some microstructural effects, Mater. Lett. 107 (2013) 370–373.

[30] J.D. Osorio, J.P. Hernández-Ortiza, A. Toro, Microstructure characterization of thermal barrier coating systems after controlled exposure to a high temperature, Ceram. Int. 40 (2014) 4663–4671.

[31] Y. Wang, W. Wu, X. Zheng, Y. Zeng, M. Ding, C. Zha, Relationship between the microstructure and thermal conductivity of plasma-sprayed ZrO2 coatings, Journal of Thermal Spray Technology, 20 (2011) 1177-1182.

[32] L. Chen, Processing, microstructures, and properties of thermal barrier coatings (TBCs) by plasma spraying (PS), in: H. Xu, H. Guo (Eds.), Thermal Barrier Coatings, Woodhead Publishing Limited, Cambridge, 2011, pp. 132-160.

[33] A. Kulkarni, A. Vaidya, A. Goland, S. Sampath, H. Herman, Processing effects on porosity-property correlations in plasma sprayed yttria-stabilized zirconia coatings, Materials and Engineering A359 (2003) 100-111.

[34] A.D. Jadhav, N.P. Padture, E.H. Jordan, M. Gell, P. Miranzo, E.R. Fuller Jr., Low-thermal-conductivity plasma-sprayed thermal barrier coatings withengineered microstructures, Acta Mater. 54 (2006) 3343–3349.

[35] S. Nath, I. Manna, J. Dutta Majumdar, Kinetics and mechanism of isothermal oxidation of compositionally graded yttria stabilized zirconia (YSZ) based thermal barrier coating, Corros. Sci., 88 (2014) 10-22.

[36] G. Pulci, J. Tirillò, F. Marra, F. Sarasini, A. Bellucci, T. Valente, C. Bartuli, High temperature oxidation and microstructural evolution of modified MCrAlY coatings, Metall. Trans. A, 45 (2014) 1401-1408.

[37] R. McPherson, Formation of metastable phases in flame- and plasma- prepared alumina, J. Mater. Sci. 8 (1973) 851–858

[38] S. Nath, I. Manna, J. Dutta Majumdar, Nanomechanical behavior of yttria stabilized zirconia (YSZ) based thermal barrier coating, Ceram. Int. 41 (2015) 5247- 5256.

[39] L. Pawlowski, P. Fauchais, Thermal transport properties of thermally sprayed coatings, Int. Mater. Rev. 37 (1992) 271-289.

[40] W.D. Kingery, Thermal conductivity: XII Temperature dependence of conductivity for single-phase ceramics, J. Am. Ceram. Soc. 38 (1955) 251-255.

[41] R.E. Taylor, X. Wang, X. Xu, Thermophysical properties of thermal barrier coatings, Surf. Coat. Technol., 120/121 (1999) 89–95.

[42] Y. Tamarin, Protective coatings for turbine blades, first ed., ASM International, Ohio, 2002.

[43] R.G. Munro, Evaluated material properties for a sintered α-alumina, J. Am. Ceram. Soc. 80 (1997) 1919–1928.

[44] X. Zhao, P. Xiao, Thermal barrier coatings on nickel superalloy substrates, Mater. Sci. Forum. 606 (2009) 1-26.

[45] P.G. Klemens, M. Gell, Thermal conductivity of thermal barrier coatings, Mater. Sci. Eng. A 245 (1998) 143–149.

[46] P.G. Klemens, Theory of the thermal conductivity of solids, in: R.P. Tye (ed.), Thermal Conductivity, Academic Press, London and New York, 1969, pp. 2–65.

[47] W. Ma, D. Macka, J. Malzbender, R. Vaßen, D. Stover, Yb_2O_3 and Gd_2O_3 doped strontium zirconate for thermal barrier coatings, J. Eur. Ceram. Soc. 28 (2008) 3071–3081.

[48] C. Poulier, D.S. Smith, J. Absi, Thermal conductivity of pressed powder compacts: tin oxide and alumina, J. Eur. Ceram. Soc., 27 (2007) 475–478.

[49] H. Yang, G.R. Bai, L.J. Thompson, J.A. Eastman, Interfacial thermal resistance in nanocrystalline yttria stabilized zirconia, Acta. Mater. 50 (2002) 2309–2317.

[50] D.S. Smith, S. Fayette, S. Grandjean, C. Martin, Thermal resistance of grain boundaries in alumina ceramics and refractories, J. Am. Ceram. Soc. 86 (2003) 105–111.

[51] P. G. Klemens, Thermal conductivity of inhomogeneous media, High Temp-High Press. 23 (1991) 241-248.

Fig. 1.   Scanning electron micrographs of the (a) YSZ, (b) Al_2O_3, and (c) CoNiCrAlY alloy feedstock powders.

Fig. 2.   X-ray diffraction profiles of the (a) YSZ, (b) Al_2O_3, and (c) CoNiCrAlY alloy feedstock powders.

Fig. 3.   Scanning electron micrographs of the cross-section of (a) 100% YSZ, (b) 70% YSZ + 30% CoNiCrAlY, (c) 50% YSZ + 50% CoNiCrAlY, (d) 30% YSZ + 70% CoNiCrAlY, and (e) 100% CoNiCrAlY composite coatings (YSZ phase in light and CoNiCrAlY phase in grey).

Fig. 4.   Scanning electron micrograph of cross-section of (a) 100% YSZ, (b) 70% YSZ + 30% Al_2O_3, (c) 50% YSZ + 50% Al_2O_3, (d) 30% YSZ + 70% Al_2O_3, (e) 100% Al_2O_3 composite coatings (YSZ phase in light and Al_2O_3 phase in dark).

Fig. 5.   Scanning electron micrograph of cross-section of fractured (a) 100% YSZ, (b) 70% YSZ + 30% CoNiCrAlY, (c) 50% YSZ + 50% CoNiCrAlY, (d) 30% YSZ + 70% CoNiCrAlY composite coatings.

Fig. 6.   Scanning electron micrograph of cross-section of fractured (a) 100% YSZ, (b) 70% YSZ + 30% Al_2O_3, (c) 50% YSZ + 50% Al_2O_3, (d) 30% YSZ + 70% Al_2O_3, (e) 100% Al_2O_3 composite coatings.

Fig. 7.   X-ray diffraction profiles of the top surface of 100% YSZ coating (plot 1), 70% YSZ + 30% CoNiCrAlY composite coating (plot 2), 50% YSZ + 50% CoNiCrAlY composite coating (plot 3), and 30% YSZ + 70% CoNiCrAlY composite coating (plot 4).

Fig. 8.   X-ray diffraction profiles of the top surface of 100% YSZ coating (plot 1), 70% YSZ + 30% Al_2O_3 composite coating (plot 2), 50% YSZ + 50% Al_2O_3 composite coating (plot 3), and 30% YSZ + 70% Al_2O_3 composite coating (plot 4), and 100% Al_2O_3 coating (plot 5).

32

Table 1. APS process parameter for the development of CoNiCrAlY/Al_2O_3/YSZ graded thermal barrier coating

Arc voltage D.C., Volt	46
Arc current D.C., Ampere	650
Primary gas (Ar) flow rate, SLPM[a]	36
Secondary gas (H_2) flow rate, SLPM[a]	10
Carrier gas (Ar) flow rate, SLPM[a]	5.1
Powder feed rate, g/min	21
Standoff distance, mm	90

[a] SLPM: standard liter per minute

Table 2. Density and porosity CoNiCrAlY/YSZ and YSZ/Al_2O_3 composite coatings

Coating	Theoretical Density (g/cm^3)	Measured Density (g/cm^3)	Relative Density (%)	Total Porosity (%)
100% YSZ	5.96	5.01	84.1	16
70% YSZ + 30% CoNiCrAlY	6.34	5.71	90.8	9.9
50% YSZ + 50% CoNiCrAlY	6.6	6.28	95.2	4.8
30% YSZ + 70% CoNiCrAlY	6.86	6.64	96.8	3.2
100 % CoNiCrAlY	7.24	7.04	97.2	2.8
70% YSZ+ 30% Al_2O_3	5.37	4.31	80.2	19.7
50% YSZ+ 50% Al_2O_3	4.97	4	80.5	19.5
30% YSZ+ 70% Al_2O_3	4.58	3.62	79	21
100% Al_2O_3	3.98	3.43	86.2	13.8

Table 3. Average coefficient of thermal expansion for CoNiCrAlY/YSZ composite coatings

Coating	Average coefficients of thermal expansion ($\times 10^{-6}/°C$)
100% YSZ	13.1
70% YSZ + 30% CoNiCrAlY	14.9
50% YSZ + 50% CoNiCrAlY	16.8
30% YSZ + 70% CoNiCrAlY	18.8
100% CoNiCrAlY	21.7

Table 4. Average coefficient of thermal expansion for Al_2O_3/YSZ composite coatings

Coating	Average coefficients of thermal expansion $(\times 10^{-6}/°C)$
100% YSZ	13.1
70% YSZ + 30% Al_2O_3	11.9
50% YSZ + 50% Al_2O_3	11
30% YSZ + 70% Al_2O_3	10.7
100% Al_2O_3	9.5

Table 5. Specific heat capacities of CoNiCrAlY/YSZ and YSZ/Al_2O_3 composite coatings

Temperature (°C)	Specific heat capacity $(Jg^{-1}K^{-1})$								
	100% YSZ [44]	70% YSZ + 30% CoNiCrAlY	50% YSZ + 50% CoNiCrAlY	30% YSZ + 70% CoNiCrAlY	100% CoNiCrAlY [45]	70% YSZ+ 30% Al_2O_3	50% YSZ+ 50% Al_2O_3	30% YSZ+ 70% Al_2O_3	100% Al_2O_3 [46]
27	0.469	0.478	0.485	0.491	0.50	0.558	0.619	0.678	0.767
200	0.542	0.544	0.546	0.548	0.55	0.686	0.782	0.877	1.021
400	0.593	0.583	0.576	0.57	0.56	0.739	0.837	0.934	1.08
600	0.618	0.603	0.594	0.584	0.57	0.79	0.904	1.019	1.19
800	0.63	0.636	0.64	0.644	0.65	0.809	0.928	1.047	1.226
1000	0.645	0.665	0.678	0.691	0.71	0.828	0.951	1.073	1.256

35

1

2

(a) Intralamellar porosity; Globular porosity; Interlamellar porosity; 2 μm
(b) Intralamellar porosity; Globular porosity; Interlamellar porosity; 2 μm
(c) Intralamellar porosity; Globular porosity; Interlamellar porosity; 2 μm
(d) Intralamellar porosity; Globular porosity; Interlamellar porosity; 2 μm
(e) Oxide stringers; 2 μm

3

4

5

6

7

8

9

10

11

12

13

14

15

16

51

17

18